

# Hyperon polarization in semi-inclusive deeply inelastic lepton-nucleon scattering at high energy

Liu Chun-xiu, Xu Qing-hua, and Liang Zuo-tang

*Department of Physics, Shandong University, Jinan, Shandong 250100, China*

## Abstract

We calculate the polarizations for different octet hyperons produced in the current fragmentation regions of the deeply inelastic lepton-nucleon scatterings  $\mu^- N \rightarrow \mu^- HX$  and  $\nu_\mu N \rightarrow \mu^- HX$  at high energy using different models for spin transfer in fragmentation processes. The results show that measurements of those hyperon polarizations should provide useful information to distinguish between different models in particular the SU(6) and the DIS pictures used frequently in the literature. We found, in particular, that measuring the polarization of  $\Sigma^+$  produced in these processes can give a better test to the validity of the different spin transfer models.

## 1. Introduction

Spin transfer in high-energy hadronization process of the fragmenting quark to the produced hadron is one of the important issues in the spin effects in hadronization processes. The problem has attracted much attention [1-12] recently. This is partly triggered by the ALEPH and OPAL measurements<sup>13,14</sup> on  $\Lambda$  polarization in  $e^+e^-$  annihilation at the  $Z^0$  pole. Compared with the theoretical calculations<sup>4,6</sup>, those data<sup>13,14</sup> seem to suggest that the simple SU(6) wave-function can be used to describe the relation between the spin of the fragmenting quark and that of the produced hyperon which contains the fragmenting quark. This is rather surprising because the energy is very high at CERN  $e^+e^-$  collider LEP and the initial quarks and antiquarks produced at the annihilation vertices of the initial  $e^+e^-$  are certainly current quarks and current antiquarks rather than the constituent quarks used in describing the static properties of hadrons using SU(6) symmetric wave-functions. A conclusive judgment of the different spin transfer models can still not be made. It is thus interesting and instructive to make further checks in experiments by making complementary measurements. For this purpose, we have made a systematic study of hyperon polarizations in different lepton-induced reactions using the SU(6) or the DIS picture. The results for  $e^+e^-$  annihilation have been presented in Ref. [11]. We now present the results for other lepton-induced reactions, such as  $\mu^-N \rightarrow \mu^-HX$  and  $\nu_\mu N \rightarrow \mu^-HX$ .

Compared with those in  $e^+e^-$  annihilations, hyperon polarizations in the current fragmentation regions of the deeply inelastic lepton-nucleon scatterings  $\mu^-N \rightarrow \mu^-HX$  and  $\nu_\mu N \rightarrow \mu^-HX$  at high energy are of particular interests for the following reasons: First, not only longitudinally but also transversely polarized quark beam can be produced in the current fragmentation regions of  $\mu^-N \rightarrow \mu^-HX$ . We can study here not only longitudinal transfer but also check whether it is the same for the transverse polarization case. Second, there is an automatic flavor separation in some cases in the deeply inelastic lepton-nucleon scatterings. For example, in the current fragmentation region of  $\nu_\mu N \rightarrow \mu^-HX$ , we have a predominant contribution from the  $u$  quark fragmentation. In  $\mu^-N \rightarrow \mu^-HX$ , we have a

combined contribution from the  $u$ ,  $d$ , and  $s$ -quarks with the corresponding weights  $\frac{4}{9}u(x)$ ,  $\frac{1}{9}d(x)$ , and  $\frac{1}{9}s(x)$ , where  $x$  is the Bjorken- $x$ , and  $q(x)$  is the number density of quark in proton. Since the  $x$  dependences of  $u(x)$ ,  $d(x)$  and  $s(x)$  are different from each other, we can tune the contributions of different flavors by choosing events in different  $x$ -region. Since different flavors contribute quite differently to the polarizations of different hyperons, we expect that the results obtained in different kinematic regions should be quite different from each other and they should also be different from those obtained in  $e^+e^-$  annihilations<sup>11</sup>. Measurements of these polarizations with high accuracy should provide us with detailed tests of different aspects of different models.

The paper is arranged as follows: In Sec. 2, we briefly summarize the calculation method of the hyperon polarization, which was outlined in Ref. [11] using  $e^+e^- \rightarrow \Lambda X$  as an example, and discuss the differences in different reactions. In Sec. 3, we present the results for the hyperon polarizations in the current fragmentation regions of the deeply inelastic scatterings off nucleon with  $\mu^-$  or  $e^-$  beam. In Sec. 4, we present our results for the hyperon polarization in the current fragmentation region of  $\nu_\mu N \rightarrow \mu^- H X$ . A brief summary of the results is given in Sec. 5.

## 2. The calculation method

The method of calculating the longitudinal polarization  $P_{H_i}$  of different hyperon  $H_i$  in the fragmentation of a longitudinally polarized quark  $q_f^0$  has been outlined in Ref. [11] using the inclusive process  $e^+e^- \rightarrow H_i + X$  as an example. The method is independent of the way how  $q_f^0$  is produced thus can certainly be applied to other processes where the longitudinally polarized fragmenting quarks are produced. Similarly, it can also be applied to processes where transversely polarized quarks are produced. We now briefly summarize the main points and discuss the differences in different reactions in the following.

We recall that, to calculate the polarization of hyperon  $H_i$ 's which are produced in the fragmentation of a polarized quark  $q_f^0$ , we should consider the  $H_i$ 's which have the following

different origins separately.

- (a) Hyperons which are directly produced and contain the fragmenting quark  $q_f^0$ ;
- (b) Hyperons which are decay products of other heavier hyperons which were polarized before their decay;
- (c) Hyperons which are directly produced but do not contain the fragmenting quark  $q_f^0$ ;
- (d) Hyperons which are decay products of other heavier hyperons which were unpolarized before their decay.

It is clear that hyperons from (a) and (b) can be polarized while those from (c) and (d) are not<sup>4,6,11</sup>. Hence, the polarization of  $H_i$  is given by

$$P_{H_i} = \frac{\sum_f t_{H_i,f}^F P_f^{(q)} \langle n_{H_i,f}^a \rangle + \sum_j t_{H_i,H_j}^D P_{H_j} \langle n_{H_i,H_j}^b \rangle}{\langle n_{H_i}^a \rangle + \langle n_{H_i}^b \rangle + \langle n_{H_i}^c \rangle + \langle n_{H_i}^d \rangle}. \quad (1)$$

Here,  $P_f^{(q)}$  is the polarization of the fragmenting quark  $q_f^0$ ;  $\langle n_{H_i,f}^a \rangle$  is the average number of the hyperons which are directly produced and contain the fragmenting quark of flavor  $f$ ;  $\langle n_{H_i,H_j}^b \rangle$  is the average number of  $H_i$  coming from the decay of  $H_j$ ,  $P_{H_j}$  is the polarization of  $H_j$  before its decay;  $\langle n_{H_i}^a \rangle (\equiv \sum_f \langle n_{H_i,f}^a \rangle)$ ,  $\langle n_{H_i}^b \rangle (\equiv \sum_j \langle n_{H_i,H_j}^b \rangle)$ ,  $\langle n_{H_i}^c \rangle$ , and  $\langle n_{H_i}^d \rangle$  are average numbers of hyperons in group (a), (b), (c), and (d), respectively;  $t_{H_i,f}^F$  is the “fragmentation polarization transfer factor” from quark  $q_f^0$  to hyperon  $H_i$ , where the superscript  $F$  stands for fragmentation;  $t_{H_i,H_j}^D$  is the “decay polarization transfer factor” from  $H_j$  to  $H_i$  in the decay process  $H_j \rightarrow H_i + X$ , where the superscript  $D$  stands for decay.

We recall that the fragmentation polarization transfer factor  $t_{H_i,f}^F$  is equal to the fraction of spin carried by the  $f$ -flavor-quark divided by the average number of quark of flavor  $f$  in the hyperon  $H_i$ <sup>4,6,11</sup>. It is different in the SU(6) or the DIS picture. The decay polarization transfer factor  $t_{H_i,H_j}^D$  is determined by the decay process. Clearly, both of them are universal in the sense that they are independent of the processes in which  $q_f^0$  and  $H_j$  are produced. They are the same in  $e^+e^-$  annihilations and in the deeply inelastic scattering with longitudinally polarized beam and/or target and in that with neutrino beam. These two factors are discussed in detail in Ref. [11]. They can be found, e.g., in table I and table II in Ref. [11], respectively.

The differences for different processes come from the polarization  $P_f^{(q)}$  of the fragmenting quark  $q_f^0$  and the average numbers  $\langle n_{H_i,f}^a \rangle$ ,  $\langle n_{H_i,H_j}^b \rangle$ ,  $\langle n_{H_i}^c \rangle$ , and  $\langle n_{H_i}^d \rangle$  for hyperon  $H_i$  of the different origins. Since the leading order hard subprocesses of these lepton-induced reactions involve only electro-weak interactions, the polarization  $P_f^{(q)}$  of the fragmenting quark  $q_f^0$  produced in these reactions can easily be calculated using the standard model of electro-weak interactions. They are in general different for  $e^+e^-$  annihilation and for deeply inelastic lepton-nucleon scatterings. They are also different in different kinematic regions in deep-inelastic scattering or for different flavors of the struck quarks. Since different flavors contribute quite differently to the polarizations of different hyperons, this makes the situation full of abundance and interesting. We will discuss them separately in next sections.

In the fragmentation process of a given flavor of quark  $q_f^0$  at a given energy, the average numbers  $\langle n_{H_i,f}^a \rangle$ ,  $\langle n_{H_i,H_j}^b \rangle$ ,  $\langle n_{H_i}^c \rangle$ , and  $\langle n_{H_i}^d \rangle$  should also be independent of the process in which  $q_f^0$  is produced. They are determined by the hadronization mechanism and should be independent of the polarization of  $q_f^0$ . But, for different reactions, the relative weights of the contributions of different flavors are different. Hence the resulting  $\langle n_{H_i,f}^a \rangle$ ,  $\langle n_{H_i,H_j}^b \rangle$ ,  $\langle n_{H_i}^c \rangle$ , and  $\langle n_{H_i}^d \rangle$  are also different in different reactions. For deeply inelastic lepton-nucleon scatterings, the relative weights are determined by the number densities of different flavors in the nucleon. This implies that the average numbers  $\langle n_{H_i,f}^a \rangle$ ,  $\langle n_{H_i,H_j}^b \rangle$ ,  $\langle n_{H_i}^c \rangle$ , and  $\langle n_{H_i}^d \rangle$  are determined by the hadronization mechanism and the structure functions of the nucleon. We emphasize here that, although neither the structure function nor the hadronization mechanism is theoretically clear yet, the form of the unpolarized parton densities in nucleon and that of the unpolarized fragmentation functions are empirically known to reasonably high accuracy. We can calculate them using the parameterizations of the structure functions and the phenomenological hadronization models. Since we are not concerned with the different correlations among the produced particles, different hadronization models lead essentially to the same results. Presently, these results can be obtained conveniently from the event generators using Monte Carlo method. We used the Lund string fragmentation model<sup>15</sup>

implemented by LEPTO<sup>16</sup> in our calculations for deeply inelastic lepton-nucleon scattering.

### 3. Hyperon polarization in the current fragmentation region of $\mu^- N \rightarrow \mu^- HX$

For sufficiently high  $Q^2$  and high total hadronic energy  $W$ , hadrons produced in the current fragmentation region in deeply inelastic lepton-nucleon scattering can be considered as a pure result of the fragmentation of the single struck quark. (Here,  $Q^2$  is the virtuality of the exchanged boson in the initial electro-weak interaction;  $W^2 = Q^2(1/x - 1) + M^2$ , and  $M$  is the nucleon mass). Hence, they can be used to study the spin effects in high-energy fragmentation processes, in particular the spin transfer from the polarized fragmenting quark to the produced hadrons. We will limit ourselves to such kinematic regions in this paper and will not discuss the cases at lower energies<sup>18,17</sup> where no distinct separation between the fragmentation results of the struck quark and that of the rest of the target nucleon is possible<sup>19</sup>. We will discuss both the case where the virtual photon exchange dominates and the case where charged weak current interaction takes place. In this section, we will discuss the first case using  $\mu^- N \rightarrow \mu^- HX$  as an example. The latter case will be discussed in Sec. 4.

In the deeply inelastic scattering  $\mu^- N \rightarrow \mu^- HX$ , the leading order hard subprocess  $\mu^- q \rightarrow \mu^- q$  is an electro-magnetic process in which a single virtual photon exchange dominates. In such subprocess, if the initial  $\mu^-$  or  $q$  is polarized or both of them are polarized, the outgoing quark can be polarized. Obviously, the polarization of the outgoing quark is dependent on the polarization of the initial  $\mu^-$ , that of  $q$ , and the scattering process. There should be a factor relating the polarization of the outgoing quark with that of the initial quark or  $\mu^-$ . This factor is usually referred as the depolarization factor. In the following, we will first briefly summarize the depolarization factor for the elementary subprocess  $\mu^- q \rightarrow \mu^- q$ , and then present the results that we obtained for hyperon polarization in the current fragmentation region of  $\mu^- N \rightarrow \mu^- HX$  using different pictures for spin transfer in the fragmentation process. We will also briefly discuss how to tune the contributions of

different flavors by choosing different  $x$  region.

### A. Depolarization factor in $\mu^- q \rightarrow \mu^- q$

The calculation of the polarization of the outgoing quark from  $\mu^- q \rightarrow \mu^- q$  is straightforward and the results can be found in different publications. For completeness, we briefly summarize the main ingredients used in the calculations and the main results which will be used in our calculations of hyperon polarization and discuss the behaviors of these results in different cases in this subsection.

We recall that the polarization of a particle system is described by the spin density matrix  $\rho$ . For the system of the incoming  $\mu^-$  and  $q$ , which are independent of each other,  $\rho$  is a direct product of that of  $q$  and that of  $\mu^-$ , which we denote by  $\rho^{(q)}$  and  $\rho^{(l)}$  respectively. The  $\rho^{(q)}$  and  $\rho^{(l)}$  are  $2 \times 2$  matrices, which is taken as the form  $\rho^{(x)} = (1 + \vec{\sigma} \cdot \vec{P}^{(x)})/2$ ; where  $\vec{\sigma}$  is the Pauli matrix and  $\vec{P}^{(x)}$  is the polarization vector of  $x (= q \text{ or } l)$ . If we know the scattering matrix  $M$  of the process, we can calculate the spin density matrix  $\rho^{out}$  for the outgoing system from the  $\rho^{in}$  for the initial system using the relation  $\rho^{out} = M \rho^{in} M^\dagger$ , or in helicity bases

$$\rho_{\lambda'_1 h'_1, \lambda'_2 h'_2}^{out} = \sum_{\lambda_1 h_1, \lambda_2 h_2} M_{\lambda'_1 h'_1, \lambda_1 h_1} \rho_{\lambda_1 h_1, \lambda_2 h_2}^{in} M_{\lambda'_2 h'_2, \lambda_2 h_2}^*, \quad (2)$$

where we use  $\lambda$  and  $h$  to denote the helicities of  $\mu^-$  and  $q$  respectively, and the prime to denote final state;  $M_{\lambda' h', \lambda h}$  is the usual helicity amplitude for the scattering process  $\mu^- q \rightarrow \mu^- q$ . We neglect the  $\mu^-$  and  $q$  mass, so that helicity is conserved, i.e.,  $M_{\lambda' h', \lambda h} \neq 0$  only if  $h' = h$  and  $\lambda' = \lambda$ . Furthermore, parity conservation requires  $M_{++,++} = M_{--,--}$  and  $M_{+-,+-} = M_{-+,-+}$ . Hence, there are only two nonzero independent  $M_{\lambda' h', \lambda h}$ 's, and they are

$$M_{++,++} = -4e^2 e_q / (1 - \cos \theta), \quad (3)$$

$$M_{+-,+-} = -2e^2 e_q (1 + \cos \theta) / (1 - \cos \theta), \quad (4)$$

where  $\theta$  is the scattering angle in the  $\mu^- q$  center of mass frame. We insert these  $M_{\lambda' h', \lambda h}$ 's

into Eq. (2), sum over the helicity of the outgoing  $\mu^-$ , and we obtain the spin density matrix for the outgoing quark as

$$\rho^{(q)out} = \begin{pmatrix} C_1 \rho_{++}^{(q)in} & C_3 \rho_{+-}^{(q)in} \\ C_3^* \rho_{-+}^{(q)in} & C_2 \rho_{--}^{(q)in} \end{pmatrix}. \quad (5)$$

Here  $C_1 = 1 + D_L(y)P_L^{(l)}$ ;  $C_2 = 1 - D_L(y)P_L^{(l)}$ ;  $C_3 = D_T(y)$ ; where  $L$  means the component parallel to the moving direction;  $y \equiv p \cdot (k - k')/p \cdot k = (1 - \cos \theta)/2$ , where  $p$ ,  $k$ , and  $k'$  are the four momenta of the incoming  $q$ ,  $\mu^-$ , and the outgoing  $\mu^-$  respectively; and

$$D_L(y) = [1 - (1 - y)^2]/[1 + (1 - y)^2]; \quad (6)$$

$$D_T(y) = 2(1 - y)/[1 + (1 - y)^2]. \quad (7)$$

In obtaining these results from Eqs. (2)-(4), we have dropped a common factor  $2e^4 e_q^2 [1 + (1 - y)^2]/y^2$ , which has no influence on the results of the polarization of the outgoing quark.

From these results, we can calculate the polarization of the outgoing  $q$  in different cases. We first discuss the case in which the initial quark is not transversely polarized, i.e.,  $\rho_{+-}^{(q)in} = \rho_{-+}^{(q)in} = 0$ . In this case, we have  $\rho_{+-}^{(q)out} = \rho_{-+}^{(q)out} = 0$ . This means that, independent of the polarization of the incoming lepton  $\mu^-$ , the outgoing quark is not transversely polarized. But, from Eq. (5), we see also that, in this case, the outgoing quark can be longitudinally polarized and the polarization is given by

$$P_L^{(q)out} = \frac{D_L(y)P_L^{(l)} + P_L^{(q)in}}{1 + P_L^{(l)}P_L^{(q)in}D_L(y)}, \quad (8)$$

where  $P_L^{(q)in} = \rho_{++}^{(q)in} - \rho_{--}^{(q)in}$  is the longitudinal polarization of the incoming quark. We see clearly that, not only the longitudinal polarization of the incoming  $q$  but also the longitudinal polarization of the incoming  $\mu^-$  can be transferred to the outgoing  $q$ . Furthermore, from Eq. (8), we see that,

$$P_L^{(q)out} = P_L^{(q)in}, \text{ for } P_L^{(l)} = 0, \quad (9)$$



which shows that the longitudinal polarization of the quark will be completely transferred to the outgoing quark, which is just the result of helicity conservation. We also see from Eq. (8) that,

$$P_L^{(q)out} = P_L^{(l)} D_L(y), \text{ for } P_L^{(q)in} = 0. \quad (10)$$

It shows that, for the scattering of a longitudinally polarized lepton on unpolarized nucleon target, the polarization of the incoming lepton can also be transferred to the outgoing quark with a reduction factor  $D_L(y)$ . Hence,  $D_L(y)$  is usually referred to as the longitudinal depolarization factor. It is interesting to see that  $D_L(y)$  is only a function of  $y$ . Its  $y$  dependence is shown by the solid line in Fig.1. We see that  $D_L(y) > 0$  for  $0 < y < 1$ , it increases with the increasing  $y$  and  $D_L(y=0) = 0$ ,  $D_L(y=1) = 1$ . We recall that, for given energy and  $Q^2$ ,  $y \propto 1/x$ . This implies that the depolarization factor  $D_L$  is large for small  $x$  but small for large  $x$ .

We denote the longitudinal polarization of the incoming nucleon by  $P_L^{(N)}$ . At a given Bjorken- $x$ , for quark of flavor  $f$ ,  $P_{fL}^{(q)in} = P_L^{(N)} \Delta q_f(x)/q_f(x)$ ; where  $q_f(x)$  and  $\Delta q_f(x)$  are the unpolarized and longitudinally polarized distribution functions of quark of flavor  $f$  inside the nucleon. Hence, we obtain the polarization of the outgoing quark of flavor  $f$  as

$$P_{fL}^{(q)out} = \frac{P_L^{(l)} D_L(y) q_f(x) + P_L^{(N)} \Delta q_f(x)}{q_f(x) + P_L^{(l)} D_L(y) P_L^{(N)} \Delta q_f(x)}. \quad (11)$$

This is the general formula which can be used to replace the  $P_f^{(q)}$  in Eq. (1) to calculate  $P_{Hi}$ . To see that  $x$  dependence of  $P_{fL}^{(q)out}$  in different cases, we show the numerical results obtained for different  $P_L^{(l)}$  and  $P_L^{(N)}$  at  $Q^2 = 10 \text{ GeV}^2$  and  $E_\mu = 500 \text{ GeV}$  using the GRSV parameterization<sup>21</sup> for parton distributions in Fig.2. From these results, we see clearly that the  $P_{fL}^{(q)out}$  are different for the different flavors, and there are considerably large differences between the results for different  $P_L^{(l)}$  and  $P_L^{(N)}$ .

Now, we discuss the second case, in which the incoming quark is transversely polarized. In this case, we have  $\rho_{++}^{(q)in} = \rho_{--}^{(q)in} = 1/2$ , and  $\rho_{+-}^{(q)in} = \rho_{-+}^{(q)in*} \neq 0$ . This means that the outgoing quark is transversely polarized. Furthermore, since  $C_3$  is a real number, the

direction of the transverse polarization with respect to the helicity frame remains the same. The magnitude of the transverse polarization of the outgoing quark is given by

$$P_T^{(q)out} = D_T(y)P_T^{(q)in}, \quad (12)$$

which is independent of the polarization of the incoming lepton  $\mu^-$ . The function  $D_T(y)$ , which is given by Eq. (7), is called transverse depolarization factor. It depends also only on  $y$  and its  $y$  dependence is given by the dashed line in Fig.1. We see that, in contrast to  $D_L(y)$ ,  $D_T(y)$  decreases with the increasing  $y$  and  $D_T(y=0) = 1$ ,  $D_T(y=1) = 0$ .

Suppose the target nucleon is transversely polarized with polarization  $P_T^{(N)}$ , at a given  $x$ , for the incoming quark of flavor  $f$ ,  $P_{fT}^{(q)in} = P_T^{(N)}\delta q_f(x)/q_f(x)$ , where  $\delta q_f(x)$  is the transversely polarized distribution function of quark of flavor  $f$ . Hence, the polarization of the outgoing quark of flavor  $f$  is given by

$$P_{fT}^{(q)out} = P_T^{(N)} \frac{\delta q_f(x)}{q_f(x)} D_T(y). \quad (13)$$

This should be used to replace the  $P_f^{(q)}$  in Eq. (1) to calculate the hyperon polarization in transversely polarized case.

## B. Hyperon polarization in the current fragmentation region in $\mu^- N \rightarrow \mu^- H X$

Having the  $P_f^{(q)}$ 's obtained in the last subsection, we can calculate  $P_{Hi}$  using Eq. (1) if we know the average numbers  $\langle n_{Hi,f}^a \rangle$ ,  $\langle n_{Hi,Hj}^b \rangle$ ,  $\langle n_{Hi}^c \rangle$ , and  $\langle n_{Hi}^d \rangle$ . We will present the results in different cases in this subsection.

### 1. $\Lambda$ polarization in $\mu^- N \rightarrow \mu^- \Lambda X$

Among all the  $J^P = \frac{1}{2}^+$  hyperons,  $\Lambda$  is most copiously produced, and it can also be measured easily through the decay channel  $\Lambda \rightarrow p\pi^-$ . Hence, till now, most of the studies [1-14,17-20] are concentrated on  $\Lambda$  polarization. However, as can be seen already in  $e^+e^-$  annihilation<sup>11</sup>, the origins of  $\Lambda$  are also most complicated. They come not only from the fragmentation

of  $u$ ,  $d$ , or  $s$ -quark, but also from the decays of many different heavier hyperons, such as,  $\Sigma^0$ ,  $\Xi^{0,-}$ ,  $\Sigma^*(1385)$ , and  $\Xi^*(1530)$ . Compared with  $e^+e^-$  annihilation, in  $\mu^-N \rightarrow \mu^-\Lambda X$  the contribution from  $u$ -quark fragmentation is much higher in particular for large  $x$ . Since  $u$  carries no spin of  $\Lambda$  in the SU(6) picture and only a small fraction of the spin of  $\Lambda$  in the DIS picture, we expect that the magnitudes of the  $P_{\Lambda(L)}$  obtained in both models for  $\mu^-N \rightarrow \mu^-\Lambda X$  should be smaller than those obtained in  $e^+e^-$  annihilation, in particular for large  $x$ . We expect also that the influences of heavier hyperon decay are larger.

Using the event generator LEPTO, we obtained the  $\langle n_{\Lambda,f}^a \rangle$ ,  $\langle n_{\Lambda,H_j}^b \rangle$ ,  $\langle n_{\Lambda}^c \rangle$ , and  $\langle n_{\Lambda}^d \rangle$  for  $\mu^-p \rightarrow \mu^-\Lambda X$ . In Fig.3, we show the different contributions in the current fragmentation region at  $E_\mu = 500\text{GeV}$ . These results are obtained for the kinematic region  $Q^2 > 5(\text{GeV}/c)^2$ ,  $10^{-4} < x < 0.2$ , and  $0.5 < y < 0.9$ . We choose this kinematic region to ensure a reasonably large  $W$  and a reasonably high polarization of the fragmenting quark. We see that the contributions from the  $s$  quark fragmentation are indeed not so dominant as that<sup>11</sup> in  $e^+e^- \rightarrow Z^0 \rightarrow \Lambda X$ . We also see that in contrast to  $s$ -quark fragmentation, the contributions from the decay of heavier hyperons in the case of  $u$  or  $d$  quark fragmentation can even be larger than those directly produced.

Using these results, we obtained  $P_{\Lambda(L)}$  in  $\mu^-p \rightarrow \mu^-\Lambda X$ , as a function of  $x_F$  shown in Fig.4 for different combinations of  $P_L^{(l)}$  and  $P_L^{(N)}$ . We see that except for the case of  $P_L^{(l)} = 0$  and  $P_L^{(N)} = 1$ ,  $P_{\Lambda(L)}$  are positive and increases with increasing  $x_F$ . Their magnitudes are significantly large, and that they are different in the SU(6) or the DIS picture in large  $x_F$  region. We also see that for  $P_L^{(l)} = 0$  and  $P_L^{(N)} = 1$ ,  $P_{\Lambda(L)}$  is negative but the magnitude is very small. This is because in this case the polarizations of the fragmenting quarks are very small and it is positive for  $u$ , but is negative for  $d$  and  $s$ . Their contributions to  $\Lambda$  polarization partly cancel with each other. Hence, we see that, to obtain a large longitudinal polarization of  $\Lambda$ , it is important to use a polarized  $\mu^-$  beam.

To show the  $x$  dependence of  $P_{\Lambda(L)}$ , we calculated also the results in the large  $x$  region ( $0.05 < x < 0.7$ ) only. The obtained results are also given in Fig.4. We see that they are significantly smaller than those in the region  $10^{-4} < x < 0.2$ . This is because for large  $x$  the

$u$  quarks play the dominant role and the contribution from  $u$  to  $\Lambda$  polarization is small.

Now we discuss the transversely polarized case. We calculate the  $\Lambda$  polarization under the assumption that the same spin transfer mechanism is true both for longitudinally and transversely polarized cases. Hence, Eq. (1) is also true for transversely polarized case, but the spin transfer factor  $t_{H_i,f}^F$  can in general be different. They are determined by the spin structure of hyperon in transversely polarized case. More precisely, in the SU(6) picture,  $t_{H_i,f}^F$  is the same for transversely and longitudinally polarized cases. But, in the DIS picture, they are determined by the helicity distribution  $\Delta q_f(x)$  in the longitudinally polarized case, but by the transversity distribution  $\delta q_f(x)$  in the transversely polarized case. Since  $\delta q_f(x)$  can in general be different from  $\Delta q_f(x)$ , the  $t_{H_i,f}^F$  in the two cases can be different from each other. Presently, the spin structure in DIS picture in transversely polarized case is still very unclear, since no measurement has been done for  $\delta q_f(x)$  yet. In order to see the order of magnitude of the polarization which we can expect for different hyperon in transversely polarized case, we made a very rough estimation by using the same  $t_{H_i,f}^F$  as those in longitudinally polarized case and  $\delta q_f(x) = \Delta q_f(x)$  in calculating  $P_{fT}^{(q)out}$  from Eq. (13). Under those approximations, the differences between the  $\Lambda$  polarization in this case and that in the longitudinally polarized case of  $P_L^{(l)}$  come only from the differences between  $D_T(y)$  and  $D_L(y)$ .

We recall that  $D_T(y)$  is larger for smaller  $y$  (see Fig.1), so we choose to study in the region  $0.1 < y < 0.7$ , in order to obtain a relatively large transverse polarization of the fragmenting quark. We also select the two groups of events in the kinematic region  $10^{-4} < x < 0.2$  and  $Q^2 > 5 \text{ (GeV/c)}^2$ , and  $0.05 < x < 0.7$  and  $Q^2 > 5 \text{ (GeV/c)}^2$ , respectively. Using the Eqs. (13) and (1), we obtained  $P_{\Lambda(T)}$  in  $\mu^- p \rightarrow \mu^- \Lambda X$ , as a function of  $x_F$  shown in Fig.5a. We see that  $P_{\Lambda(T)}$  is negative but its magnitude is relatively small (of the order of 0.02).

We note that longitudinal  $\Lambda$  polarization has been measured<sup>18</sup> by HERMES Collaboration at HERA in  $e^+ p \rightarrow e^+ \Lambda X$  at 27.5 GeV/c. However, we can not compare our results shown in Fig.4 with the HERMES data, since the energy in that experiment is rather low. At that energy, no separation between the fragmentation of the struck quark and that of

the rest of the target proton is possible. A detailed discussion of this problem is given in Ref. [22].

## 2. Polarization of other hyperons in $\mu^-p \rightarrow \mu^-HX$

From the results that we obtained in the last subsection, we see that, because of the large contributions from  $u$  and  $d$  quark fragmentation in  $\mu^-p \rightarrow \mu^-\Lambda X$ , the contributions from the decay of heavier hyperons are large and the  $\Lambda$  polarization in transversely polarized case is very small. Since the contributions of different flavors to the spins of the  $J^P = (3/2)^+$  hyperons are unknown yet in the DIS picture and only models are known to calculate the spin transfer in their decay processes, there are considerably large theoretical uncertainties in the results that we can obtain yet. On the other hand, as we have already seen<sup>11</sup> in studying  $e^+e^- \rightarrow Z^0 \rightarrow HX$ , the origins of other  $J^P = (1/2)^+$  hyperons, i.e.,  $\Sigma$  and  $\Xi$ , are rather clear. The decay contributions are much smaller than the corresponding contributions for  $\Lambda$  production. Hence, the uncertainties in the theoretical calculation in this case can be significantly reduced. We thus continue to study the polarization of these  $J^P = (1/2)^+$  hyperons in  $\mu^-N \rightarrow \mu^-HX$  in the following. We note in particular that, in current fragmentation region of  $\mu^-p \rightarrow \mu^-X$ ,  $u$ -quark fragmentation plays the dominant role. Since the fractional contribution of  $u$  quark to the spin of  $\Sigma^+$  is large, the resulting  $\Sigma^+$  polarization in the current fragmentation region of  $\mu^-p \rightarrow \mu^-\Sigma^+X$  should be significantly larger than that for  $\Lambda$ .

Furthermore, also because of the large contribution of  $u$ -quark fragmentation, the ratio of the production rate of  $\Sigma^+$  to that of  $\Lambda$  in the current fragmentation region of  $\mu^-p \rightarrow \mu^-HX$  should be significantly higher than from that in  $e^+e^-$  annihilation<sup>11</sup>, in particular for large  $x_F$  where hyperon polarization should be studied. This can easily be checked using the event generator LEPTO. In Fig.6a, we show the ratios of the production rate of  $\Sigma^+$  to that of  $\Lambda$  as function of  $x_F$ . We see that the ratio increases with increasing  $x_F$ , and is already very close to 1 at  $x_F = 0.8$ . Therefore, the statistics in studying  $\Sigma^+$  should not be much worse than

that for  $\Lambda$ .

In addition to the directly produced, there is only one decay contribution for  $\Sigma^+$  from  $\Sigma^*(1385)$ . In Fig.6b, we show the two different contributions to  $\Sigma^+$  in the events where  $10^{-4} < x < 0.2$ . We see that the decay contribution from heavier hyperon is very small. It takes only about 3% in the current fragmentation region. Hence, the uncertainties in the calculations for  $\Sigma^+$  are much smaller than those for  $\Lambda$  and the study of  $\Sigma^+$  polarization should provide us with a good complementary test to different spin transfer pictures.

Using the event generator LEPTO, we calculated the different average numbers  $\langle n_{\Sigma^+,f}^a \rangle$ ,  $\langle n_{\Sigma^+,H_j}^b \rangle$ ,  $\langle n_{\Sigma^+}^c \rangle$ , and  $\langle n_{\Sigma^+}^d \rangle$ . We insert them into Eq. (1) and obtain  $P_{\Sigma^+(L)}$  for different combinations of  $P_L^{(l)}$  and  $P_L^{(N)}$  as a function of  $x_F$  in Fig.7. We see that, because of the dominance of the contribution from  $u$ -quark fragmentation, and because  $u$ -quark contributes very largely to the spin of  $\Sigma^+$ , the obtained  $P_{\Sigma^+(L)}$  is in general large and positive in  $\mu^-p \rightarrow \mu^-\Sigma^+X$ . We see also that the difference between the results based on the two different pictures are also larger compared with those for  $\Lambda$  and these properties are more significant for the events with  $0.05 < x < 0.7$ . The results again show that it is important to use a polarized  $\mu^-$  beam to obtain a large longitudinal polarization of  $\Sigma^+$ .

Similar to  $\Lambda$ , we also made a rough calculation of the transverse polarization  $P_{\Sigma^+(T)}$  of  $\Sigma^+$  under the same assumption and/or approximations. The obtained results are shown in Fig.5b. We see that, compared with those for  $\Lambda$ , the magnitude of  $P_{\Sigma^+(T)}$  is much larger.  $P_{\Sigma^+(T)}$  has similar properties as  $P_{H_i(L)}$ . It increases with increasing  $x_F$ , and the results obtained in the different pictures are significantly different from each other in particular at  $0.05 < x < 0.7$ . We see also that  $P_{\Sigma^+(T)}$  at  $0.05 < x < 0.7$  is larger compared with that at  $10^{-4} < x < 0.2$ . Hence, we expect that the measurement of  $P_{\Sigma^+(T)}$  should provide useful information on the transverse polarization transfer in high-energy fragmentation processes.

At the same time, we also make similar calculations for other octet hyperons, i.e.,  $\Sigma^-$ ,  $\Xi^0$  and  $\Xi^-$ . The obtained results are shown in Figs.8, 9 and 10. We also performed the same calculations for reactions using neutron target. Because of the difference caused by the charge factor in the electromagnetic interactions which make the  $u$  (or  $d$ ) contributions

in the case of the neutron target be higher (lower) than that of  $d$  (or  $u$ ) in the case of proton target, there is no exact  $u$ - $d$  exchange symmetry in the results obtained in the two cases. We can not obtain the results for hyperon in the case of neutron from those in the case of proton by making an interchange of  $u$  and  $d$ . But the qualitative features can be obtained in this way. Hence, we expect that measuring  $\Sigma^-$  polarization in  $\mu^- n \rightarrow \mu^- \Sigma^- X$  can give us useful information for spin transfer in fragmentation process.

#### 4. Hyperon polarization in the current fragmentation region of $\nu_\mu N \rightarrow \mu^- H X$

Compared with  $e^+e^-$  annihilation and  $\mu^-p$  deeply inelastic scattering, the deep-inelastic scattering process  $\nu_\mu N \rightarrow \mu^- H X$  has the following two distinct advantages. First, the magnitude of the polarization of the fragmenting quark is large. In  $\nu_\mu N \rightarrow \mu^- H X$ , the leading order hard subprocess is  $\nu_\mu q \rightarrow \mu^- q$ , which is a charged current weak interaction with the exchange of the virtual  $W^+$ . According to the standard model for weak interaction, the charged current weak interaction selects only left-handed quarks (right-handed antiquark), so the polarization of the fragmenting quarks is  $P_f^{(q)} = -1$ . Second, there is an automatic flavor separation. For sufficiently high  $Q^2$  and high total hadronic energy  $W$ , the dominant contributions in the current fragmentation region of  $\nu_\mu N \rightarrow \mu^- H X$  come from the fragmentation of the fully polarized  $u$  quarks. Thus, measuring the polarization of the hyperon in this reaction should be able to provide us with a very sensitive test to different models for the spin transfer in the fragmentation process.

With the aid of LEPTO event generator, we calculated  $\Lambda$  and  $\Sigma^+$  longitudinal polarizations in the current fragmentation region of  $\nu_\mu p \rightarrow \mu^- H X$  at  $E_\nu = 500$  GeV and  $Q^2 > 5(\text{GeV}/c)^2$ . We find out that, the contributions from the decay of different heavier hyperons to  $\Lambda$  are very large. This can be seen in Fig.11. We see that the decay contribution are even larger than those directly produced. We see also that there are significant contributions from the decay of  $\Lambda_c$  and other charm-baryons. In particular in the region of  $x_F < 0.4$ , they are larger than the contributions from the other origins. Since the decay spin transfer factor  $t_{H_i, H_j}^D$  is

model dependent and the polarizations of these heavier hyperons are unclear, these results imply that there are large theoretical uncertainties in calculating  $P_{\Lambda(L)}$ , in particular from the treatment of  $\Lambda_c$  and other charm baryon decays. We thus made a very rough estimation for  $P_{\Lambda(L)}$  using the  $t_{\Lambda, H_j}^D$  given in table II in Ref. [11] as input. For  $\Lambda_c$ , we simply take the fragmentation polarization transfer from the  $c$  quark to  $\Lambda_c^+$  is 1, and the decay polarization transfer factor for  $\Lambda_c^+ \rightarrow \Lambda l^+ \nu_l$  is also taken as 1, i.e.,  $t_{\Lambda_c^+, c}^F = 1$  and  $t_{\Lambda, \Lambda_c^+}^D = 1$ . The obtained results are shown in Fig.12a. To show the influence of  $\Lambda_c^+$  decay, we show also the results obtained by taking  $t_{\Lambda, \Lambda_c^+}^D = 0$ . We see that, in the case of  $t_{\Lambda, \Lambda_c^+}^D = 0$ ,  $\Lambda$  polarization  $P_{\Lambda(L)}$  is very small. This is because the contributions from the decay of  $\Sigma^*$  and  $\Xi^*$  to  $\Lambda$  polarization are negative but other contributions are positive, and they partly cancel with each other. We see also that  $P_{\Lambda(L)}$  decreases with increasing  $x_F$  at  $x_F < 0.5$  and increases with increasing  $x_F$  at  $x_F > 0.5$ . This is because the contributions from the decay of  $\Sigma^*$  and  $\Xi^*$  are dominant at  $x_F < 0.5$  and decrease at  $x_F > 0.5$ . These results obtained in the case of  $t_{\Lambda, \Lambda_c^+}^D = 1$  differs largely from those in the case of  $t_{\Lambda, \Lambda_c^+}^D = 0$ . In this case  $P_{\Lambda(L)}$  is still negative, but the magnitude of  $P_{\Lambda(L)}$  is much larger than that in the case of  $t_{\Lambda, \Lambda_c^+}^D = 0$ . The decrease with increasing  $x_F$  at  $x_F < 0.4$  and the increase with increasing  $x_F$  at  $x_F > 0.4$  is due to the contributions from  $\Lambda_c^+$  decay are dominant at  $x_F < 0.4$  and decrease at  $x_F > 0.4$ .

In contrast to  $\Lambda$ , from Fig.12b and 12d, we see that the contributions from the decay of heavier strange hyperons and charm-baryons to  $\Sigma^+$  are very small. The contributions from the decay of  $\Sigma^*$  containing the fragmenting  $u$  quark only take about 1%, and that those from the decay of  $\Lambda_c$  and other charm-baryons take only about 8%. Therefore the theoretical uncertainties in calculating  $\Sigma^+$  polarization are small. Furthermore, because of the dominance of the  $u$  quark fragmentation, we expected that the  $\Sigma^+$  production rate should be relatively high. This can easily be seen in Fig.12 or Fig. 13 where we show the ratio of the production rate of  $\Lambda$  to that of  $\Sigma^+$ . The result shows that the ratio increases with the increasing  $x_F$ , and reaches about 1.6 at  $x_F = 0.8$ . Hence, the statistics for  $\Sigma^+$  is not less than that for  $\Lambda$  in the current fragmentation region of  $\nu_\mu p \rightarrow \mu^- \Lambda / \Sigma^+ + X$ .

Inserting these results into Eq.(1) we obtain the  $\Sigma^+$  polarization shown in Fig.12b, where



the contributions from the decay of charm-baryons are not taken into account. We see that  $\Sigma^+$  polarization is negative and its magnitude is very large and increases with increasing  $x_F$ , and the difference between the results based on the two different pictures is quite significant. Hence measuring  $P_{\Sigma^+(L)}$  in the current fragmentation region of  $\nu_\mu p \rightarrow \mu^- \Sigma^+ X$  should be very validity to distinguish the different pictures for spin transfer in high-energy fragmentation processes.

## 5. Summary

We calculated the polarizations for different octet hyperons produced in the current fragmentation regions of the deeply inelastic lepton-nucleon scatterings  $\mu^- N \rightarrow \mu^- H X$  and  $\nu_\mu N \rightarrow \mu^- H X$  for sufficiently large  $Q^2$  and  $W^2$  using different models for spin transfer in high-energy fragmentation processes. We discussed in detail the contributions from different sources including those from the decay of different heavier hyperons. Our results show that measurements of these hyperon polarizations should provide useful information to distinguish between different models in particular the SU(6) and the DIS pictures used frequently in the literature. We found in particular that decay contributions to  $\Lambda$  are very important in  $\mu^- N \rightarrow \mu^- \Lambda X$  and  $\nu N \rightarrow \mu^- \Lambda X$  and have to be taken into account in calculating the  $\Lambda$  polarizations in these reactions. We found also that measuring the polarizations of  $\Sigma^+$  in  $\mu^- p \rightarrow \mu^- \Sigma^+ X$  or  $\nu_\mu p \rightarrow \mu^- \Sigma^+ X$  can give a much better test to the validity of the different models than that obtained by measuring  $\Lambda$  in the corresponding processes not only because the magnitudes of  $P_{\Sigma^+}$  and the differences between different models are much larger than that of  $P_\Lambda$  but also because the theoretical uncertainties are much smaller in calculating the former. Measuring  $P_{\Sigma^+(T)}$  in transversely polarized case should be able to give an useful check whether in high-energy fragmentation process the polarization transfer mechanisms are the same for both the longitudinally polarized and transversely polarized cases.

We thank Li Shi-yuan, Xie Qu-bing and other members in the theoretical particle physics

group of Shandong University for helpful discussions. This work was supported in part by the National Science Foundation of China (NSFC) and the Education Ministry of China.

## REFERENCES

1. See, for example, Refs.[2-12] and the references given there.
2. R.L. Jaffe, and Ji Xiangdong, Phys. Rev. Lett. **67** , 552 (1991); Nucl. Phys. **B 375**, 527 (1992).
3. M. Burkardt and R.L. Jaffe, Phys. Rev. Lett. **70**, 2537 (1993).
4. G.Gustafson and J.Häkkinen, Phys. Lett. **B 303**, 350 (1993).
5. R.L. Jaffe, Phys. Rev. **D 54**, R6581 (1996).
6. C. Boros, and Liang Zuo-tang, Phys. Rev. **D 57**, 4491 (1998).
7. A. Kotzinian, A. Bravar, D. von Harrach, Eur. Phys. J. **C 2**, 329-337 (1998).
8. D. Ashery, H. J. Lipkin, Phys. Lett. **B 469**, 263 (1999); and hep-ph/0002144.
9. B.Q. Ma, I. Schmidt, and J.J. Yang, Phys. Rev. **D 61**, 034017 (2000).
10. M. Anselmino et al, Phys. Lett. **B 481**, 253 (2000).
11. Liu Chun-xiu and Liang Zuo-tang, Phys. Rev **D 62**, 094001 (2000).
12. B.Q. Ma, I. Schmidt, J. Soffer, and J.J. Yang, Phys. Rev. **D 62**, 114009 (2000); **D63**, 037501 (2001).
13. ALEPH Collaboration; D. Buskulic et al., Phys. Lett. **B 374**,319 (1996).
14. OPAL Collaboration; K. Ackerstaff et al., Euro. Phys. J. **C 2**, 49-59 (1998).
15. B. Anderson, G. Gustafson, G. Ingelman, and T. Sjöstrand, Phys. Rep. **97**, 31 (1983).
16. G. Ingelman, LEPTO version 6.1, Proc. Physics at HERA", Eds. W. Buchmueller et al., DESY Hamburg 1992, vol.3 p. 1366; G Ingelman, A.Edin, J.Rathsman, LEPTO 6.5, Comp. Phys. Comm. **101**, 108 (1997).
17. NOMAD Collaboration, P. Astier et al., Nucl. Phys. **B 588**, 3 (2000).

- 18. HERMES Collaboration, A. Airapetian et al., hep-ex/9911017.
- 19. We note that at HERMES or NOMAD energies, the total hadronic squared,  $W^2$ , is typically of the order of  $10 \text{ (GeV)}^2$ . Hence,  $W$  is only of several GeV. In this case, no separation of the fragments of the scattered quark and those of the rest of the nucleon is possible. Hence, the contamination from usual target fragments to the current fragmentation is very high.
- 20. E665 Collaboration, M.R. Adams *et al.*, Euro. Phys. J. **C 17**, 263 (2000).
- 21. M. Glück, E. Reya, M. Stratmann, W. Vogelsang, Phys. Rev. **D 63**, 094005 (2001).
- 22. Liu Chun-xiu *et al.*, in preparation.

# FIGURES

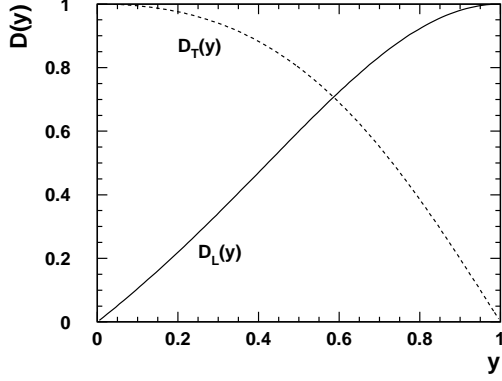


Fig. 1. Depolarization factors  $D_L(y)$  and  $D_T(y)$  as functions of  $y$  in  $\mu^- q \rightarrow \mu^- q$  for the scattered quark.

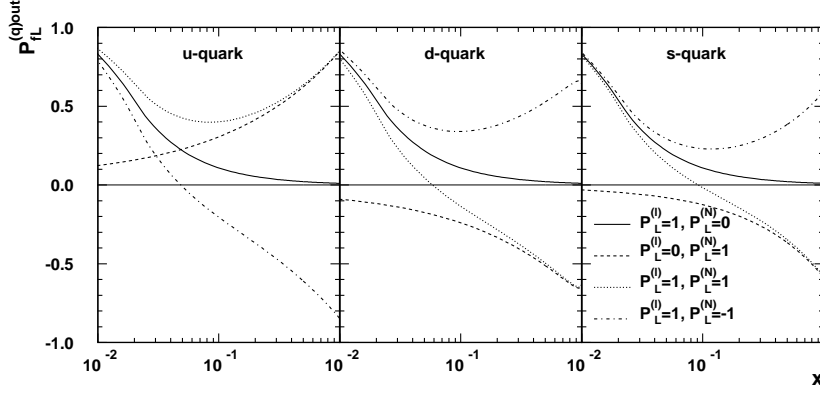


Fig. 2. The  $x$  dependences of the polarization  $P_{fL}^{(q)out}$  of the outgoing scattered  $q_f$  in  $\mu^- p \rightarrow \mu^- X$  for different combinations of  $P_L^{(l)}$  and  $P_L^{(N)}$  at  $Q^2 = 10 \text{ (GeV/c)}^2$  and  $E_\mu = 500 \text{ GeV}$ .

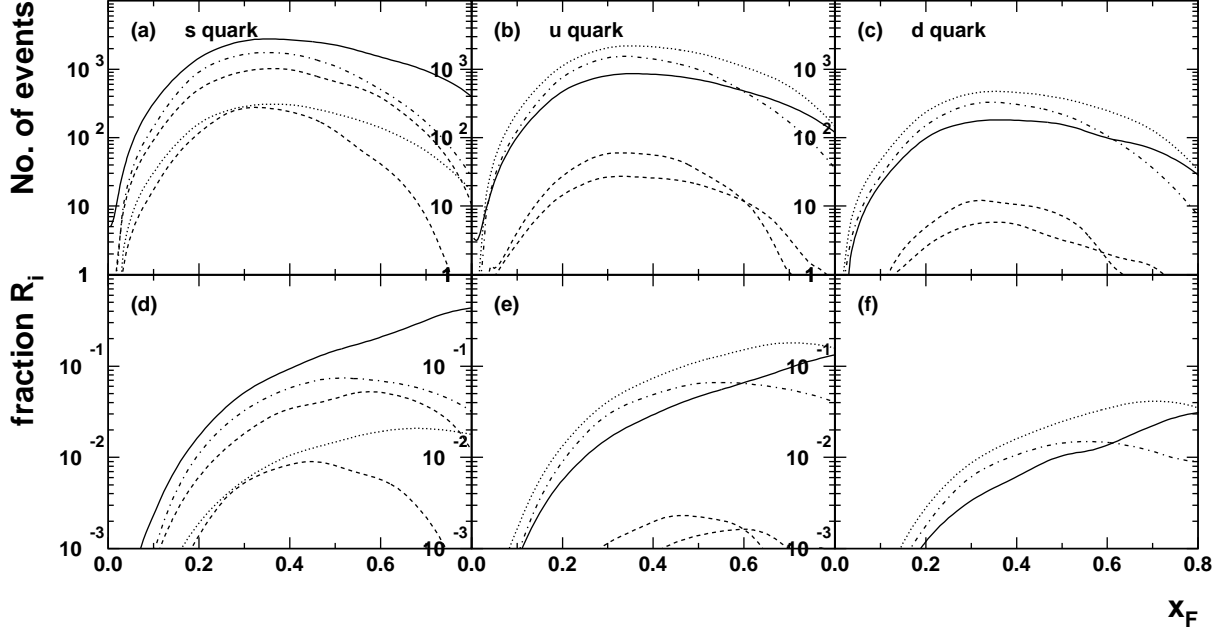


Fig. 3. Different contributions to  $\Lambda$  in events originating from the  $s$ ,  $u$ , or  $d$  quark fragmentation as functions of  $x_F = 2p_z^*/W$  in  $\mu^- p \rightarrow \mu^- \Lambda X$  at  $E_\mu = 500\text{GeV}$ . In (a)-(c), we see the five types of contributions from  $s$ ,  $u$ , or  $d$  quark respectively. The solid line denotes those which are directly produced and contain the fragmenting quark; the *upper* dashed, *lower* dashed, dotted, and dash-dotted lines respectively denote those from the decay of  $\Xi$ ,  $\Xi^*$ ,  $\Sigma^0$ , and  $\Sigma^*$  which contain the fragmenting quark. In (d)-(f), we see the fractions  $R_i$  which are the ratios of the corresponding contributions to the sum of all different contributions.

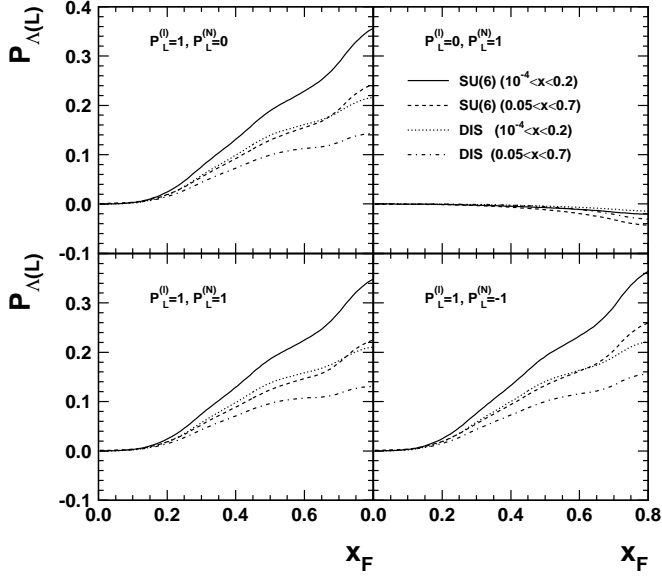


Fig. 4. Longitudinal polarization  $P_{\Lambda(L)}$  of  $\Lambda$  as a function of  $x_F$  for the different combinations of  $P_L^{(l)}$  and  $P_L^{(N)}$ . The solid and dotted lines are respectively the results based on the SU(6) and the DIS pictures for the events with  $10^{-4} < x < 0.2$ ; the dashed and dash-dotted lines are the corresponding results for the events with  $0.05 < x < 0.7$ .

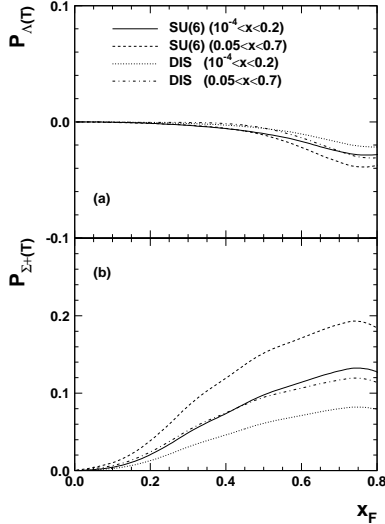


Fig. 5. Transverse polarization of  $\Lambda$  and  $\Sigma^+$ ,  $P_{\Lambda(T)}$  and  $P_{\Sigma^+(T)}$ , as functions of  $x_F$ .

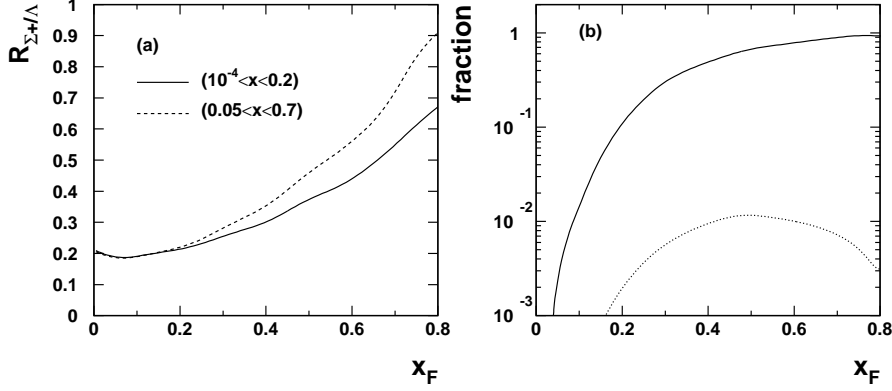


Fig. 6. (a): Ratio of the production rate of  $\Sigma^+$  to that of  $\Lambda$  as a function of  $x_F$ . The solid and dashed lines are respectively the results for the events where  $10^{-4} < x < 0.2$  and the events where  $0.05 < x < 0.7$ . (b): Different contributions to  $\Sigma^+$  in  $\mu^-p \rightarrow \mu^-\Sigma^+X$  at  $E_\mu = 500$  GeV. The solid and dashed lines are respectively the contributions which are directly produced and contain the fragmenting quark and those which are originate from the decay of polarized heavier hyperons.

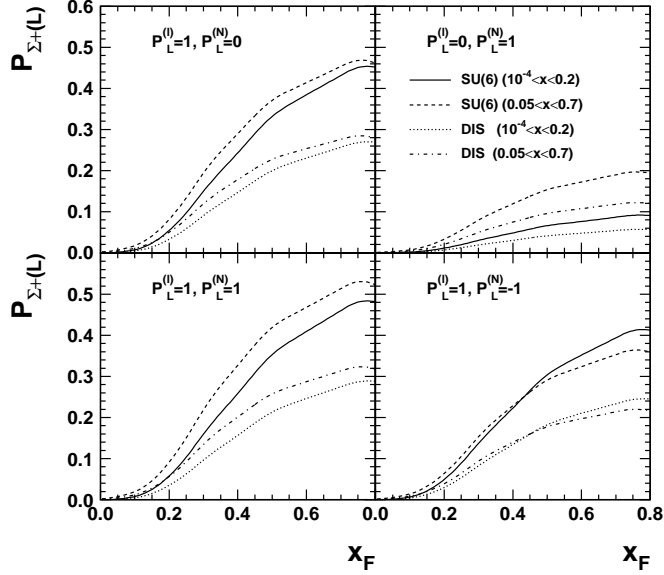


Fig. 7. Longitudinal polarization  $P_{\Sigma^+(L)}$  of  $\Sigma^+$  in the current fragmentation region of  $\mu^-p \rightarrow \mu^-\Sigma^+X$  as a function of  $x_F$ .



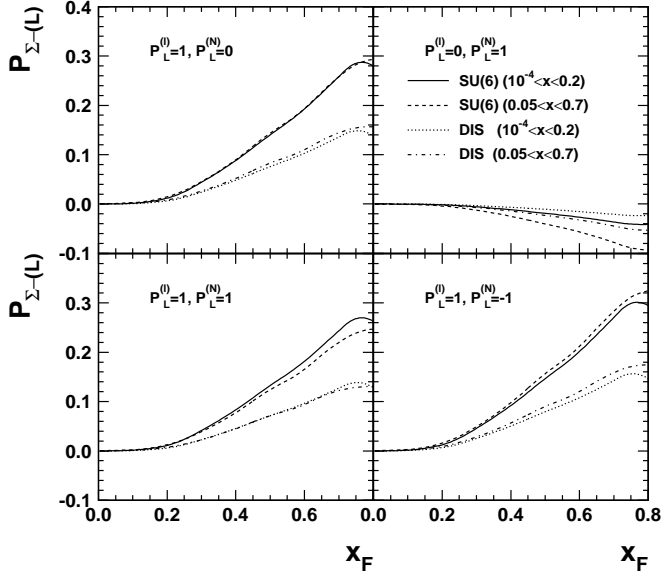


Fig. 8. Longitudinal polarization  $P_{\Sigma^-(L)}$  of  $\Sigma^-$  in the current fragmentation region of  $\mu^- p \rightarrow \mu^- \Sigma^- X$  as a function of  $x_F$ .

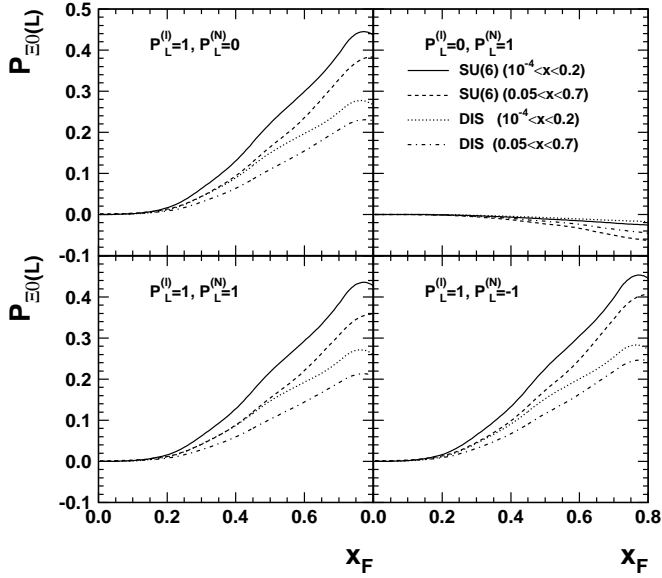


Fig. 9. Longitudinal polarization  $P_{\Xi^0(L)}$  of  $\Xi^0$  in the current fragmentation region of  $\mu^- p \rightarrow \mu^- \Xi^0 X$  as a function of  $x_F$ .

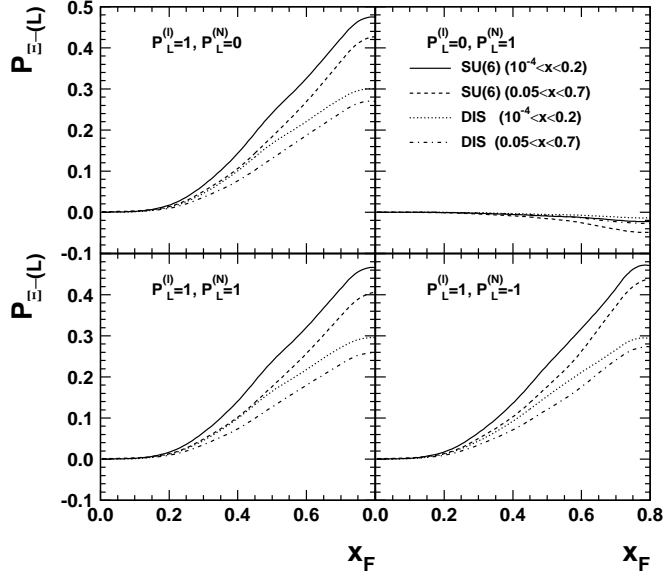


Fig. 10. Longitudinal polarization  $P_{\Xi^-(L)}$  of  $\Xi^-$  in the current fragmentation region of  $\mu^- p \rightarrow \mu^- \Xi^- X$  as a function of  $x_F$ .

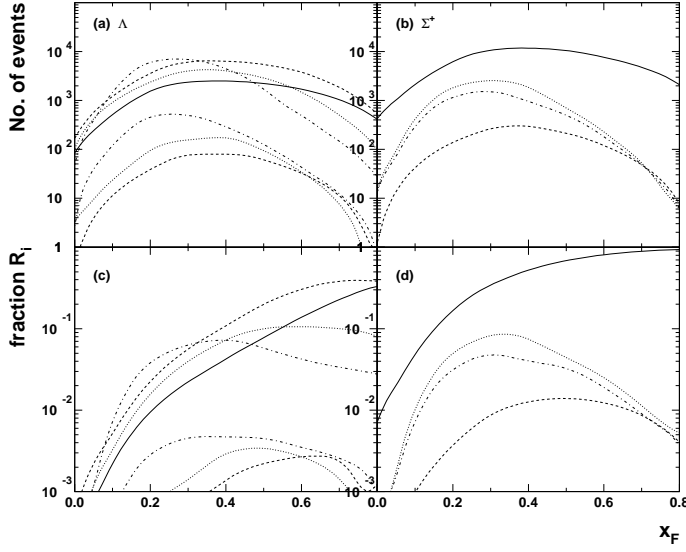


Fig. 11. Different contributions to  $\Lambda$  or  $\Sigma^+$  in the fragmentation of  $u$ , and  $c$  quarks as functions of  $x_F$  in the current fragmentation region of  $\nu_\mu p \rightarrow \mu^- H X$  at  $E_\nu = 500$  GeV. In (a), we see the seven types of contributions to  $\Lambda$ . The solid, *upper* dashed, *upper* dotted, *lower* dashed, and *lower* dotted lines denote those which are directly produced or from the decay of  $\Sigma^0$ ,  $\Sigma^*$ ,  $\Xi$ , and  $\Xi^*$  that contain the fragmenting  $u$  quark; the *upper* dash-dotted and *lower* dash-dotted lines denote those from the decay of  $\Lambda_c^+$  and other charm-baryons. In (b), we see the four types of contributions to  $\Sigma^+$  in the fragmenting  $u$  and  $c$  quark events. Here, the solid and dashed lines denote those which are directly produced and contain the fragmenting  $u$  quark and those from the decay of  $\Sigma^*$  that contain the fragmenting  $u$  quark respectively; the dotted and dash-dotted lines denote those from the decay of  $\Lambda_c^+$  and other charm-baryons. In (c) and (d), we see the fractions  $R_i$  which are the ratios of the corresponding contributions to the sums of all these different contributions for  $\Lambda$  and  $\Sigma^+$  respectively.

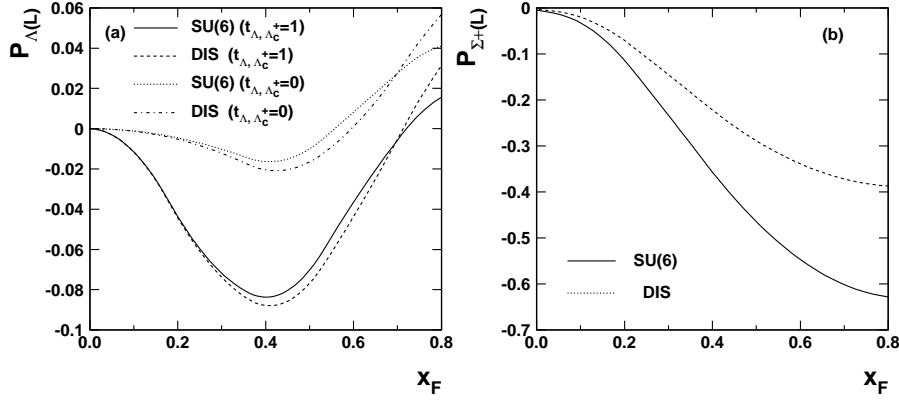


Fig. 12. Longitudinal polarizations of  $\Lambda$  and  $\Sigma^+$  in the current fragmentation region of  $\nu_\mu p \rightarrow \mu^- H X$ . In (a), the solid and dashed lines are respectively the results based on the SU(6) and DIS pictures at  $t_{\Lambda, \Lambda_c}^D = 1$ ; the dotted and dash-dotted lines are respectively the results based on the SU(6) and DIS pictures at  $t_{\Lambda, \Lambda_c}^D = 0$ . In (b), the solid and dashed lines are respectively the results obtained based on the SU(6) and DIS pictures, where the decay of charm-baryons are not taken into account.

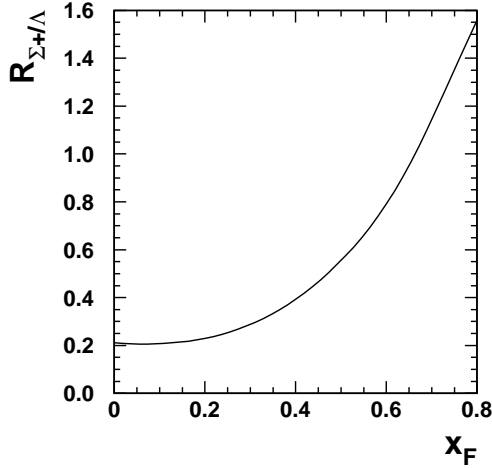


Fig. 13. The ratio of the production rate of  $\Sigma^+$  to that of  $\Lambda$  as a function of  $x_F$  in the current fragmentation region of  $\nu_\mu p \rightarrow \mu^- H X$ .

## Figure captions

Fig.1: Depolarization factors  $D_L(y)$  and  $D_T(y)$  as functions of  $y$  in  $\mu^-q \rightarrow \mu^-q$  for the scattered quark.

Fig.2: The  $x$  dependences of the polarization  $P_{fL}^{(q)out}$  of the outgoing scattered  $q_f$  in  $\mu^-p \rightarrow \mu^-X$  for different combinations of  $P_L^{(l)}$  and  $P_L^{(N)}$  at  $Q^2 = 10 \text{ (GeV/c)}^2$  and  $E_\mu = 500 \text{ GeV}$ .

Fig.3: Different contributions to  $\Lambda$  in events originating from the  $s$ ,  $u$ , or  $d$  quark fragmentation as functions of  $x_F = 2p_z^*/W$  in  $\mu^-p \rightarrow \mu^-\Lambda X$  at  $E_\mu = 500 \text{ GeV}$ . In (a)-(c), we see the five types of contributions from  $s$ ,  $u$ , or  $d$  quark respectively. The solid line denotes those which are directly produced and contain the fragmenting quark; the *upper* dashed, *lower* dashed, dotted, and dash-dotted lines respectively denote those from the decay of  $\Xi$ ,  $\Xi^*$ ,  $\Sigma^0$ , and  $\Sigma^*$  which contain the fragmenting quark. In (d)-(f), we see the fractions  $R_i$  which are the ratios of the corresponding contributions to the sum of all different contributions.

Fig.4: Longitudinal polarization  $P_{\Lambda(L)}$  of  $\Lambda$  as a function of  $x_F$  for the different combinations of  $P_L^{(l)}$  and  $P_L^{(N)}$ . The solid and dotted lines are respectively the results based on the SU(6) and the DIS pictures for the events with  $10^{-4} < x < 0.2$ ; the dashed and dash-dotted lines are the corresponding results for the events with  $0.05 < x < 0.7$ .

Fig.5: Transverse polarization of  $\Lambda$  and  $\Sigma^+$ ,  $P_{\Lambda(T)}$  and  $P_{\Sigma^+(T)}$ , as functions of  $x_F$ .

Fig.6:(a): Ratio of the production rate of  $\Sigma^+$  to that of  $\Lambda$  as a function of  $x_F$ . The solid and dashed lines are respectively the results for the events where  $10^{-4} < x < 0.2$  and the events where  $0.05 < x < 0.7$ . (b): Different contributions to  $\Sigma^+$  in  $\mu^-p \rightarrow \mu^-\Sigma^+X$  at  $E_\mu = 500 \text{ GeV}$ . The solid and dashed lines are respectively the contributions which are directly produced and contain the fragmenting quark and those which are originate from the decay of polarized heavier hyperons.

Fig.7: Longitudinal polarization  $P_{\Sigma^+(L)}$  of  $\Sigma^+$  in the current fragmentation region of  $\mu^p \rightarrow \mu^-\Sigma^+X$  as a function of  $x_F$ .

Fig.8: Longitudinal polarization  $P_{\Sigma^-(L)}$  of  $\Sigma^-$  in the current fragmentation region of  $\mu^- p \rightarrow \mu^- \Sigma^- X$  as a function of  $x_F$ .

Fig.9: Longitudinal polarization  $P_{\Xi^0(L)}$  of  $\Xi^0$  in the current fragmentation region of  $\mu^- p \rightarrow \mu^- \Xi^0 X$  as a function of  $x_F$ .

Fig.10: Longitudinal polarization  $P_{\Xi^-(L)}$  of  $\Xi^-$  in the current fragmentation region of  $\mu^- p \rightarrow \mu^- \Xi^- X$  as a function of  $x_F$ .

Fig.11: Different contributions to  $\Lambda$  or  $\Sigma^+$  in the fragmentation of  $u$ , and  $c$  quarks as functions of  $x_F$  in the current fragmentation region of  $\nu_\mu p \rightarrow \mu^- H X$  at  $E_\nu = 500$  GeV. In (a), we see the seven types of contributions to  $\Lambda$ . The solid, *upper* dashed, *upper* dotted, *lower* dashed, and *lower* dotted lines denote those which are directly produced or from the decay of  $\Sigma^0$ ,  $\Sigma^*$ ,  $\Xi$ , and  $\Xi^*$  that contain the fragmenting  $u$  quark; the *upper* dash-dotted and *lower* dash-dotted lines denote those from the decay of  $\Lambda_c^+$  and other charm-baryons. In (b), we see the four types of contributions to  $\Sigma^+$  in the fragmenting  $u$  and  $c$  quark events. Here, the solid and dashed lines denote those which are directly produced and contain the fragmenting  $u$  quark and those from the decay of  $\Sigma^*$  that contain the fragmenting  $u$  quark respectively; the dotted and dash-dotted lines denote those from the decay of  $\Lambda_c^+$  and other charm-baryons. In (c) and (d), we see the fractions  $R_i$  which are the ratios of the corresponding contributions to the sums of all these different contributions for  $\Lambda$  and  $\Sigma^+$  respectively.

Fig.12: Longitudinal polarizations of  $\Lambda$  and  $\Sigma^+$  in the current fragmentation region of  $\nu_\mu p \rightarrow \mu^- H X$ . In (a), the solid and dashed lines are respectively the results based on the SU(6) and DIS pictures at  $t_{\Lambda, \Lambda_c^+}^D = 1$ ; the dotted and dash-dotted lines are respectively the results based on the SU(6) and DIS pictures at  $t_{\Lambda, \Lambda_c^+}^D = 0$ . In (b), the solid and dashed lines are respectively the results obtained based on the SU(6) and DIS pictures, where the decay of charm-baryons are not taken into account.

Fig.13: The ratio of the production rate of  $\Sigma^+$  to that of  $\Lambda$  as a function of  $x_F$  in the current

fragmentation region of  $\nu_\mu p \rightarrow \mu^- H X$ .